International Journal of Theoretical and Applied Mathematics
2025, Vol. 11, No. 4, pp. 55-64
https://doi.org/10.11648/j.ijtam.20251104.11

Research Article

Mathematical Modelling of Host – Pathogen – Drug Interaction Dynamics and Immune Modulation in Viral Infection

Paul Kipkurgat Choge, Titus Kiplimo Rotich*, Wesley Cheruiyot Koech

Department of Mathematics, Physics and Computing, Moi University, Eldoret, Kenya

Abstract

Viral infections target the same immune system cells which fight against the infection, significantly curtailing the capacity of the body to fight associated diseases. Once the virus successfully infects a cell, it uses the same highly proliferating immune host cells to multiply, and enjoy host immunity. With the absence of HIV treatment, available chemotherapy is used to boost immune system, inhibit infection, and disrupt the assembling of viral materials during reproduction. This is achieved by use of Highly Active Anti-Retroviral Therapy (HAART) which contains immune proliferation boosters, reverse transcriptase inhibitors (RTI) and Protease Inhibitors (PI) components. In this paper, a host-pathogen-drug interaction triangle mathematical model is formulated to depict the effect of chemotherapeutic control on reproductive ratio. A SEIR paradigm was used and modified to show differentiated adaptive immune T and B cells, and a viral load compartment. Reproductive ratio R_0 was computed using the next generation matrix, together with its elasticity to control parameters. It was found that in absence of any controls, the reproductive ratio $R_0 = 0.659$ and as C_E increases, this value reduces with elasticity of $E_{CE} = -1.298$ at the critical drug concentration at effect site of $C_E(t) = 0.72$ of the dose. Simulation revealed that the most sensitive component of HAART is the PI at elasticity of $E_\pi = -1.573$, followed by the drug potency to directly kill viral materials ω, closely followed by the drug potency to kill infected immune cells ψ and lastly by the RTI's ability to prevent infection η. In conclusion, correct composition of HAART and consist dosing to maintain therapeutic window concentration reduces the viral load, boosts the immune system to normalcy, and generates a pool of memory cells, ready for immediate attack in the subsequent re-infection. This restores the health of People Living with HIV/AIDS (PLWHA), reduces the force of infection of susceptible cells and consequently reduce disease incidence rate across the population.

Keywords

Pharmacokinetics, Therapeutic Window, Chemotherapeutic Potency, Compartmental Modelling, Reproductive Ratio, Next Generation Matrix, Parameter Sensitivity, Protease Inhibitors

1. Introduction

Human beings are in constant interaction with their environment, and some of these interactions adversely affect their health through exposure to contaminated food, polluted air, physical injury, psychological stress, and intrinsic physio-

*Corresponding author: drtkchebion@gmail.com (Titus Kiplimo Rotich)

Received: 8 October 2025; **Accepted:** 25 October 2025; **Published:** 3 December 2025

logical dysfunctions. Ill health arises when normal physiological functions are disrupted, either through pathogenic invasion or autoimmune malfunction. This makes the use of drugs for treatment, or to relieve symptoms, or to prevent infection and to restore physiological balance inevitable. The dosages in administration of drugs depends on the age, body weight, bioavailability and severity of the disease. These are monitored through blood plasma concentrations, side effect tracking or by use of pharmacokinetics and pharmacodynamics [1].

Pharmacokinetics plays a critical role in determining the onset, duration and intensity of a drug's effect [2]. This acumen helps in understanding the time course of the concentration of a drug in the body and how these varied concentrations impact the therapeutic results [3]. Pharmacodynamics is the branch of pharmacology that studies the biochemical and physiological effects of drugs and their mechanisms of action in the body [4].

The use of mathematical modeling in pharmacology helps in describing the absorption, distribution, metabolism, and excretion of drugs together with its effects on the target site. Mathematical model simulation helps predict, optimize drug dosages, improves the drug designs and help monitor anticipation of side effects. These are vital parameters in clinical decision making. In this paper, the focus is on compartmental modeling to show the relationship between the drug concentration and the effect at the site of action [5]. Mathematical models have been used to describe the relationship between drug dose or concentration in blood plasma and the physiological effect at the target site. The connection dynamics between glucose homeostasis, insulin kinetics and the pharmacological effects of antidiabetic therapeutic agents on the treatment of diabetes mellitus was best described by pharmacokinetic and pharmacodynamics models [6]. This model also captured the delayed and feedback regulated responses in glucose insulin systems.

The parameters used in pharmacokinetic and pharmacodynamics integration models showed that the maximum plasma concentration (C_{max}) determines how quickly and how much the drug is bioavailable in the blood stream [7]. The pharmacokinetic and pharmacodynamics model was used to accurately predict the lung growth curves when using data from a clinical study for testing growth hypotheses of the lung tumor against clinical data [8]. Analyses of various mathematical compartmental models were employed to predict drug dosage and efficacy incorporating genetic, physiological and environmental factors. Modeling has therefore helped to optimize therapeutic outcomes while minimizing adverse effects [9].

Pharmacokinetic and pharmacodynamics models' analysis have proven to be very useful in establishing rational dosage regimens of antimicrobial agents in human medicine [10]. In addition, the simultaneous processes of drug release and in vivo absorption, distribution, metabolism and elimination processes following different administration routes have shown that bioavailability drug solubility, permeability, gastrointestinal transit time and systemic absorption can be accurately predicted [11]. This was done using a system of ordinary differential equations to model the chemotherapeutic pharmacokinetics and pharmacodynamics derived from reaction kinetics.

In this study, the adaptive immune system is structured into T and B cells, in order to evaluate their distinct roles and contributions to pathogen clearance and control. The formulation of a tripartite model facilitated the inclusion of PK/PD components in determining the critical therapeutic threshold, together with the analysis of the efficacy of specific ingredients of HAART, besides monitoring the viral load. This is the contribution of this study to existing related literature.

2. Materials and Methods

In order to formulate the mathematical model, the description of the modeling domain is first defined as follows: After the invasion of a pathogen, the human system mounts a cascade of biochemical defense mechanism reactions to neutralize the pathogens. The first line of defense in the innate immune system, which is unspecific and always ready. The first line of defense involves natural killer cells, dendritic cells, phagocytes among others. The second line of defense in the adaptive immune system, which involves antigen-specific T and B cells, which are activated on interaction with the antigen. Once activated, the T and B cells undergo clonal differentiation and rapid proliferation of cells which induce apoptosis, lysis of infected cells, and activate other cells involved in clearing the infection [12]. Once the pathogens are cleared, memory cells are retained for effective response in an event of subsequent infection [13].

The use of chemotherapy supports the interaction of the immune system and the pathogens. Specially formulated antigens and other materials can be used in vaccination to develop and boost the immune system against the specific pathogen [14].

2.1. Mathematical Modeling of Immune System

The interaction of the immune system, pathogens and chemotherapy involve highly complex pathways. For the purpose of understanding the immune response to viral infection, a simplified model is formulated using compartmental paradigm. The immune and pathogen cell density per unit volume is categorized and clustered into different compartments and the transition rates due to cause and effect across the compartments is monitored. Six categories of cells will be considered, namely; Na ïve phagocytes, exposed latent phagocytes, Infected Phagocytes, activated T-Cells, activated B-Cells and free viral pathogens, denoted by S, E, I, T, B, V respectively.

The following variables will be used to denote the cell population of each cluster. Let $S(t)$ denote the concentration

of naive immune cells, $E(t)$ is used to denote the concentration of immune cells exposed to viral materials but not infected. These are the cells that become activated and differentiate to produce antibodies or transform to other antigen specific immune cells. A collection of successfully infected cells which have viral materials integrated into their DNA and are denoted by $I(t)$. The differentiated adaptive immune system cells are monitored using the variables $T(t)$ and $B(t)$ for the cytotoxic T cells and B-Cells respectively. The viral load determining the level of infection is monitored using the variable $V(t)$. Additional compartment to model the presence of chemotherapy is introduced. The variable indicating the concentration of drugs is here denoted by $C_p(t)$ and $C_E(t)$, where the subscript denoted the plasma and the effect site concentration respectively. The drug concentration is modeled using two-compartment PK-PD model and since chemotherapy is not part of the immune system cells, its model is treated separately and the concentration at the target site is incorporated into the cel dynamics model to account for the physiological effect of the drug.

2.2. Model Parameters

The following parameters describe the transition rates between compartments. New naive susceptible immune cells are produced from the bone marrow at a constant rate of λ and naturally die at a rate of μ_1. In presence of viral particles, antigen presenting cells bind to the antigen and expose the naive immune cells at a rate of ξ. The exposed cells have a natural death of μ_2 and if the immune system does not prevent infection (penetration of viral materials into the cells), they become infected at a rate of β. Exposed cells differentiate and undergo clonal selection and expansion into effector cells (tailored to fight the specific virus directly) B cells or (effector cells that respond by indirectly killing infected cells) T cells. The proportion $(1-\vartheta)$ of exposed immune cells become activated and undergo clonal differentiation, and the remaining complement ϑ remain inactivated. The proportion ε of activated cells proliferate into T cells at the rate of β_1 and other proportion γ differentiate into B cells at a rate of β_2. The T cells cause accelerated elimination of infected cells (both T and B cells) at a rate π. Proliferated T cells reproduce at a rate of δ while the B cells reproduce at a rate of ρ and are eliminated due to natural attrition or become used up at a rate of μ_4. Infected cells die naturally at a rate of μ_3 and additional accelerated death rate of $(\alpha+\tau+\psi c_E)$ is experienced due to apoptosis α, lysis at a rate τ and by chemotherapeutic effect at a rate of ψC_E which depends on the drug efficacy c_E.

Infected cells with viral genome integrated in the host DNA, burst after lysis and produce viral materials at a burst size of K with τ as the bursting rate. Free viral materials are assumed to enter into our bodies at a constant rate of θ and naturally die at a constant rate of μ_5. Viral materials can however be eliminated by chemotherapy at accelerated death rate of ω and additional viruses are killed by B cells at a rate of φ.

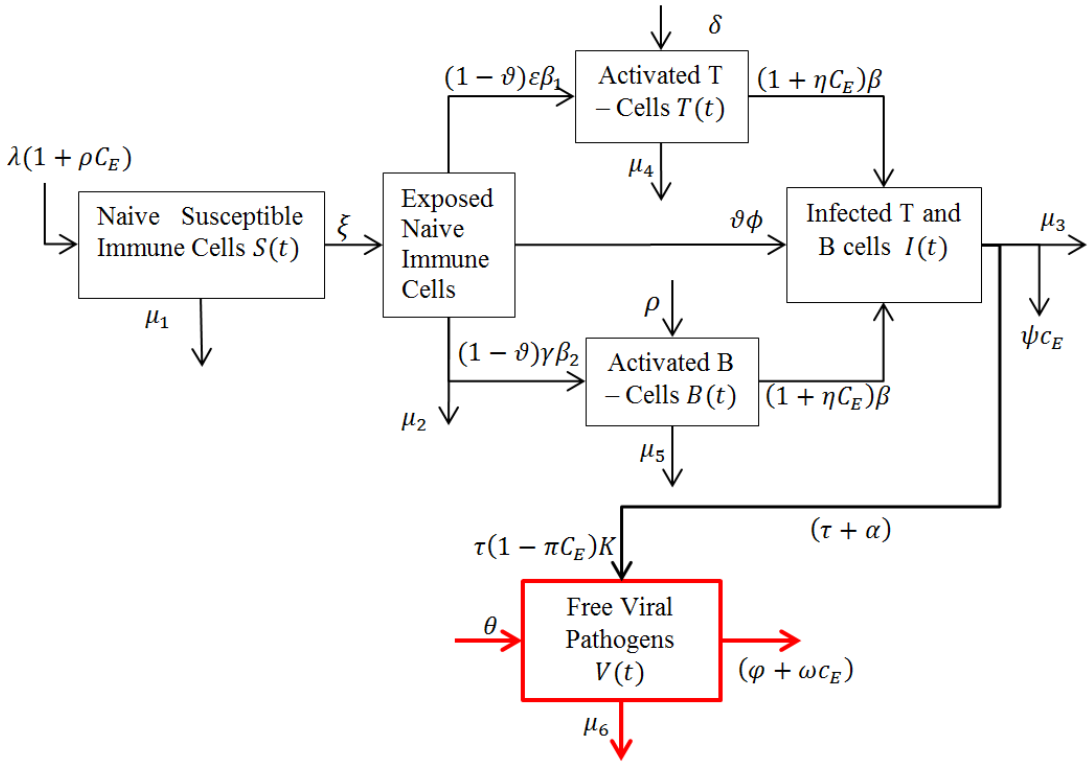

Figure 1. *Flow chart showing Innate and Adaptive immune response to pathogenic infection.*

The drug concentration at the effect site denoted by C_E is hereby coupled with the system of cell dynamics to show the effect of chemotherapy on the treatment of the pathogens. It is here assumed that chemotherapy C_E has a triple effect in the body. One by reducing the infection rate of exposed naive immune cells by the factor η. This reduces the infection rate β to $(1-\eta C_E)\beta$. Secondly, chemotherapy augments elimination of infected cells with a drug efficacy rate of ψ and by boosting the immune response of lysis τ, apoptosis α and B – Cell viral removal φ by the πC_E which depend on drug concentration. The number of infected cells eliminated by chemotherapy will be $\psi C_E I$, which depends on the drug concentration C_E. Thirdly, chemotherapy is assumed to play the role of killing or dissolving free viral materials at a rate of ω multiplied by the drug concentration in the effect site C_E. The interaction of variables through transition parameters described is represented schematically by the flow chart in Figure 2. The rectangular shapes represent the compartments, while the arrows represent the transition of cells from one compartment to the other due to change in status.

2.3. Model Equations of Immune Response with Chemotherapy

From the flow chart and the descriptions of variables and parameters above, the following system of differential equations are formulated, to account for the changes in each compartment.

$$\frac{dS}{dt} = \lambda(1+\rho C_E) - \xi SV - \mu_1 S \tag{1}$$

$$\frac{dE}{dt} = \xi SV - (1-\vartheta)[\varepsilon\beta_1 + \gamma\beta_2]E - \vartheta\phi E - \mu_2 E \tag{2}$$

$$\frac{dI}{dt} = \beta(1-\eta C_E)(B+T) + \vartheta\phi E - (\alpha+\tau)TI - \psi C_E I - \mu_3 I \tag{3}$$

$$\frac{dT}{dt} = \delta + (1-\vartheta)\varepsilon\beta_1 E - \beta(1-\eta C_E)T - \mu_4 T \tag{4}$$

$$\frac{dB}{dt} = \rho + (1-\vartheta)\gamma\beta_2 E - \beta(1-\eta C_E)B - \mu_5 B \tag{5}$$

$$\frac{dV}{dt} = \theta + \tau(1-\pi C_E)KI - \varphi BV - \omega C_E V - \mu_6 V \tag{6}$$

This model was analyzed for its stability at disease free equilibrium and the effect of chemotherapy on the value of reproductive ratio R_0.

2.4. Disease Free Equilibrium and Reproductive Ratio

Define disease free equilibrium as $Eq^0 = (S^0, E^0, I^0, T^0, B^0, V^0) = (S^0, 0, 0, 0, 0, 0)$, where $S^0 = \frac{\lambda}{\mu_1}$. Using the next generation matrix method [15], the infection classes are identified as $x = (E, I, T, B, V)^T$. The new infection terms matrix F and the transition matrix V are defined as;

$$F = \begin{pmatrix} 0 & 0 & 0 & 0 & \xi S^0 \\ 0 & 0 & 0 & 0 & 0 \\ 0 & 0 & 0 & 0 & 0 \\ 0 & 0 & 0 & 0 & 0 \\ 0 & 0 & 0 & 0 & 0 \end{pmatrix}, \text{ and the transition matrix}$$

$$V = \begin{pmatrix} a_{11} & 0 & 0 & 0 & 0 \\ -\vartheta\phi & a_{22} & -a_{23} & -a_{24} & 0 \\ -(1-\vartheta)\varepsilon\beta_1 & 0 & a_{33} & 0 & 0 \\ -(1-\vartheta)\varepsilon\beta_2 & 0 & 0 & a_{44} & 0 \\ 0 & a_{52} & 0 & 0 & a_{55} \end{pmatrix}, \text{ where}$$

$a_{11} = (1-\vartheta)[\varepsilon\beta_1 + \gamma\beta_2] + \vartheta\phi + \mu_2$, $a_{22} = \mu_3 + \psi C_E$, $a_{23} = a_{24} = (1-\eta C_E)\beta$ $a_{33} = \mu_4 + \beta(1-\eta C_E)$, $a_{44} = \mu_5 + \beta(1-\eta C_E)$ $a_{52} = \tau(1-\pi C_E)K$ and $a_{55} = \mu_6 + \omega C_E$.

The reproductive ratio is obtained as the dominant spectral radius of the next generation matrix

$$R_0 = \sigma(FV^{-1}) \tag{7}$$

This yields the reproductive ratio of,

$$R_0 = \frac{\xi\tau(1-\pi C_E)K\lambda}{\mu_1(\mu_6+\omega C_E)} \cdot \frac{(1-\vartheta)\beta(1-\eta C_E)(a_{44}\varepsilon\beta_1 + a_{33}\gamma\beta_2)}{a_{11}a_{22}a_{33}a_{44}} \tag{8}$$

It is noted that the chemotherapeutic concentration at the effect site C_E appears in the basic reproductive ratio in two ways; one is to augment the elimination rate μ_3 of infected cells and that μ_6 of free viruses. The public health targets the control strategies of reducing R_0 to values less than one. In this model, the chemotherapeutic control appears in the reproductive ratio in four ways; one by augmenting the elimination rates μ_3, of infected cells, increasing the elimination rate μ_6 of viruses, thirdly by reducing the infectivity β of naive cells, and lastly by reducing the burst size production of new viruses. The elasticity of this multifaceted control strategy is of interest, to determine the target composition of HAART.

2.5. Sensitivity Analysis of C_E on R_0

Sensitivity of parameters describe how significant a unit change in a constraint causes changes in reproductive ratio. As a control measure, it is expected that chemotherapy causes a negative change in reproductive ratio. For any parameter p, the elasticity of R_0 with respect to the parameter is defined as;

$$E_p = \frac{p}{R_0}\frac{\partial R_0}{\partial p} = \frac{\partial \ln R_0}{\partial \ln p} \tag{9}$$

From the definition of the reproductive ratio R_0 in equation (8), the elasticity of the control parameter C_E is computed as;

$$E_{C_E} = C_E\left(\frac{M}{\Pi} + \frac{\eta\beta}{a_{33}} + \frac{\eta\beta}{a_{44}} - \left(\frac{\psi}{a_{22}} + \frac{\omega}{a_{55}}\right)\right) \quad (10)$$

where $\Pi = (1-\vartheta)\varepsilon\beta_1 a_{22}a_{44} + (1-\vartheta)\gamma\beta_2 a_{22}a_{33} + \vartheta\phi a_{33}a_{44}$, and $M = (1-\vartheta)\varepsilon\beta_1\psi a_{44} + (1-\vartheta)\gamma\beta_2\psi a_{33} - \vartheta\phi\eta\beta(a_{33} + a_{44})$.

3. Model Simulation Results

In order to visualize the model, the following parameters were obtained from literature as indicated and some of them were estimated for the purpose of simulating the model dynamics. The initial values of variables are taken as follows. For a disease-free equilibrium, we have; $S^0 = 1200, T^0 = 0, B^0 = 0$, and the value of the other parameters are presented in Table 1 below.

Table 1. *Parameter Values for Model Simulation.*

Symbol	Description	Value	Source
λ	Production rate of immune cells (T, B and others)	2	[16]
ξ	Rate of exposure of viral materials presented by APC	0.2	[17]
μ_1	Natural death rate of naïve immune system cells	0.135	[18]
μ_2	Natural death rate of exposed undifferentiated immune cells	0.135	[18]
μ_3	Natural death rate of infected undifferentiated immune cells	0.45	[17]
μ_4	Natural death rate of T-Cells	0.45	[19]
μ_5	Natural death rate of B cells	0.745	[20]
μ_6	Natural death rate of viruses	12	[18]
α	Accelerated death rate due to (programmed retirement) apoptosis	0.035	[17]
ψ	Drug potency/killing rate of infected cells by drugs	[0 – 1]	Variable
C_E	Drug concentration at the effect site	[0 – 1]	Variable
η	Drug efficacy to prevent successful infection	[0 – 1]	Variable
ρ	Drug potency to boost Haematopoiesis	[0 – 1]	Variable
ω	Drug potency to eliminate free viral materials	[0 – 1]	Variable
π	Therapeutic protease inhibition potency to reduce viral burst size	[0 – 1]	Variable
θ	Initial entry of viruses from the environment	0.00033	[18]
β	Progression rate of exposed differentiated immune cells to infection state	0.052	[17]
ϕ	Progression rate of exposed naive immune cells to infection state	0.0422	[15]
φ	Accelerated death of viruses due to the killing effect by B-Cells	0.025	[20]
K	Viral burst size (number of viruses produced by an infected cell)	100	[18]
τ	Bursting rate of infected cells due to lysis triggered by T cells	0.02	[21]
β_1, β_2	Activation rate of differentiation and cloning of T cells and B cells	0.75	[19]
δ	Basal recruitment rate of T cells even after clearance of infection	2	[19]
σ	Basal production rate of B cells (before and after viral clearance)	3	[20]
ε	Proportion of cells which differentiate to T cells	0.5	[19]
γ	Proportion of activated cells which differentiate to B cells	0.5	[20]
ϑ	Proportion of cells which fail to be activated and not differentiated	0.2	[21]

3.1. Disease Free Equilibrium

This equilibrium represents a normal situation when an individual is not exposed to any disease. In this case, there are no initial differentiated cells specialized for a particular disease. This state only exists at the beginning of simulation of an individual who has never had exposure to a particular pathogen before. DFE, is simulated, in absence of chemotherapy; that $E(t) = I(t) = T(t) = B(t) = V(t) = 0$ with chemotherapeutic parameters $C_E = 0$. This scenario is depicted in Figure 2. It is noted that the naive cell population increases gradually, then settles at a constant value after all transient dynamics die, meanwhile the population of other cell types remain zero throughout the simulation.

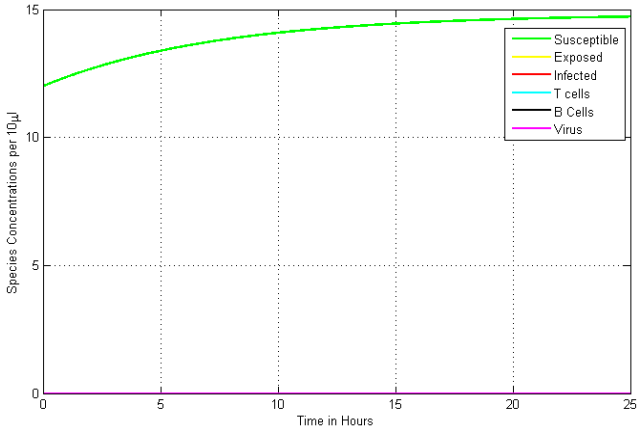

Figure 2. *Naive Cell dynamics at Disease Free Equilibrium.*

3.2. Chronic Equilibrium Point

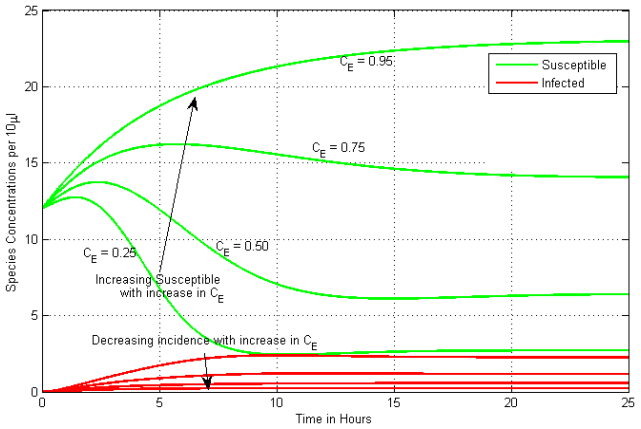

Figure 4. *Treatment model showing the effect of C_E on S(t) and I(t).*

From Figure 6 it is noted that increase if the concentration

When an individual is exposed to the virus, and successfully infected, the immune system is not able to clear the virus completely, due to the in vivo immunity. However, the viral load can be eliminated to undetectable levels. With the help of chemotherapy, the resolution of the viral infestation is achieved faster and more effectively. The simulation of these two scenarios is depicted in Figure 5 and Figure 6 respectively.

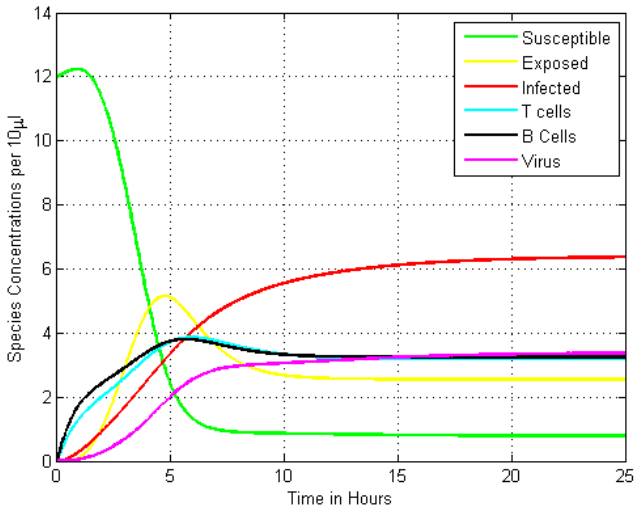

Figure 3. *Infection state Cell Dynamics in absence of Treatment.*

The cell populations at Chronic equilibrium without therapy is settling at $(S, E, I, T, B, V) = (78.15, 254.96, 636.90, 319.58, 324.51, 337.17)$. Using the parameter values in Table 1 above, the computation of R_0 in absence of chemotherapy yields $R_0 = 0.659$.

of $C_E(t)$ has a fourth fall effect as explained in section 3.4.6, that is; boosting production of stem cells by ρ, kill free virus by a proportion ω, augment protease inhibition reducing reproduction of viral materials by π, prevent infection through reverse transcription inhibition by η, and kill infected cells through lysis by the proportion ψ. The elasticity of these parameters is necessary to determine the direction and effort of intervention.

3.3. Pharmacokinetic Modeling of Optimal Chemotherapeutic Dosage C_E

The observance of chemotherapy and maintenance of desired concentration at effect site depends on dosage behaviour. The concentration of chemotherapy at effect site can be modelled using two compartment pharmacokinetics model. This model describes the concentration of drugs at the central compartment $C_p(t)$ and that of peripheral compartment at the effect site as $C_E(t)$. The transfer rates of drugs across the two

compartments are described by the parameters $k_{ij}, i,j = 0,1,2$ as shown in Figure 4 [22]. The transfer rates k_{01}, k_{10}, k_{12}, k_{21} are first order kinetics of drug distribution, where; $C_p(t)$ is the concentration in the central compartment; $C_E(t)$ is the concentration in the peripheral compartment; $k_{01}$is the rate constant for dose administered to the body at the $t = 0$; k_{10} is the rate constant for eliminationfrom the central compartment; k_{12} is the rate constant for drug transfer from the central compartment to the peripheral compartment; k_{21} is the rate constant for drug transfer from the peripheral compartment to the central compartment [23].

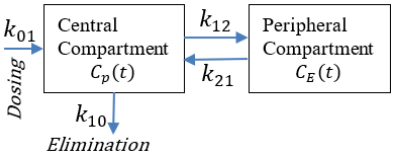

Figure 5. *Two - Compartmental model of drug PK.*

The target of PK and PD studies is to achieve a desired drug concentration at the effect site. Using first order kinetics, the equations representing the drug concentration dynamics from the two compartment PK model is given by;

$$\frac{dC_P}{dt} = k_{01}C_P - k_{12}C_P + k_{21}C_E - k_{10}C_P \tag{11}$$

$$\frac{dC_E}{dt} = k_{12}C_P - k_{21}C_E \tag{12}$$

The drug concentration at the effect site $C_E(t)$, that lead to the treatment is the parameter that matters in the chemotherapeutic model. It is this parameter that determines the measure of the killing rate or physiological effect desired. The viral killing rate of drugs, or the drug efficacy on receptors depends on the drug concentration at the site $C_E(t)$ and the half saturation constant KC_{50} given by the relation;

$$Drug_{Killing\ rate} = \left(\frac{Kmax C_E(t)}{(KC_{50}+C_E(t))}\right)V_{load} \tag{13}$$

The concentration of the drug is varied in the interval $[0,1]$ denoting 100% concentration in the effect site depending on the individual requirements. These requirements include body fluid volume, age, body size, weight, elimination rate among others as discussed earlier. In matrix form, equation (11) and (12) is given by;

$$\begin{pmatrix} C_p' \\ C_E' \end{pmatrix} = \begin{pmatrix} k_{00} & k_{21} \\ k_{12} & -k_{21} \end{pmatrix}\begin{pmatrix} C_p \\ C_E \end{pmatrix} \tag{14}$$

where $k_{00} = k_{01} - k_{12} - k_{10}$. Using diagonalization principles and direct integration by the method of integrating factor, we obtain the solution of equation (14) as;

$$C_P(t) = \frac{1}{\lambda_1-\lambda_2}e^{b_0 t}C_{P_0} + \frac{\lambda_1\lambda_2}{(\lambda_1-\lambda_2)k_{12}}e^{b_1 t}C_{E_0} \tag{15}$$

$$C_E(t) = \frac{k_{12}}{\lambda_1-\lambda_2}\left[e^{d_0 t}C_{P_0} + \frac{1}{k_{12}}e^{d_1 t}C_{E_0}\right] \tag{16}$$

where $b_0 = \left(\lambda_1 e^{\lambda_1 t} - \lambda_2 e^{\lambda_2 t}\right), b_1 = \left(e^{\lambda_2 t} - e^{\lambda_1 t}\right), d_0 = \left(e^{\lambda_1 t} - e^{\lambda_2 t}\right), d_1 = \left(\lambda_1 e^{\lambda_2 t} - \lambda_2 e^{\lambda_1 t}\right)$ while C_{P_0} and C_{E_0} are initial concentrations of drug in the blood plasma and in the effect site respectively.

Simulation of PK model for HAART for an average adult is illustrated below. HAART drug concentration for a single dose shows a drop in the concentration in the plasma drops from 100% down to zero, as the concentration in the effect site rises from zero to a peak of 87% of the drug initial dosage in approximately one hour. This concentration is then eliminated so that if no other dose is administered, the concentration is cleared in 24 hours as depicted in Figure 6.

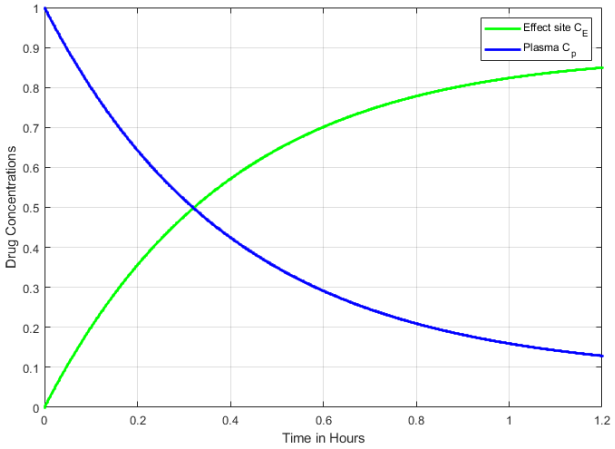

Figure 6. *Drug Concentration at Plasma and Peripheral site in the first 1 hour.*

Multiple dosing as guided by the medical expert (after considering individual characteristics and the severity of the infection) maintains the drug concentration at the effect site within therapeutic window whose simulation yields an average of $C_E(t) = 0.72$.

3.4. Sensitivity of Control Parameters to R_0

As discussed in section 3.7. sensitivity of parameters is necessary to guide control strategies, and from the data in Table 1., the following are the sensitivities of various parameters to the reproductive ratio. For various values of $C_E(t)$, the following are computations of reproductive ratio, and the sensitivity of various control parameters.

From Table 2, it is noted that elasticity E_{C_E} of drug concentration becomes increasingly negative as concentration $C_E(t)$ increases. This means that the elasticity HAART components which include; protease-inhibitor potency E_π is

negative and increasing in magnitude as drug concentration increases. This means improving PI proportion π yields large reductions in R_0.

Elasticity of viral clearance E_ω is negative but it has a smaller effect than π. The effect of drug direct killing of infected cells ψ is negative but very small in this parameter regime. Similarly, the effect of RTI is small negative. The role of HAART in boosting immune cells proliferation ρ is seen to have a positive elasticity, therefore larger ρ increases the abundance of T and B cells, and consequently increases their direct effect through apoptosis and lysis, whose effect contributes to direct reduction of R_0.

Table 2. *Control parameter Values and Elasticities to Reproductive Ratio.*

Drug Conc. $C_E(t)$	**Reproductive Ratio** (R_0)	**Parameter Elasticities**						
		(E_{C_E})	(E_ρ)	(E_τ)	(E_π)	(E_ψ)	(E_η)	(E_ω)
0.00	0.659	~0.0	+0.001	+1.00	−0.001	−0.000	−0.000	−0.000
0.25	0.604	−0.134	+0.175	+1.00	−0.269	−0.004	−0.018	−0.017
0.50	0.498	−0.511	+0.297	+1.00	−0.734	−0.005	−0.036	−0.034
0.72	0.368	−1.298	+0.379	+1.00	−1.573	−0.005	−0.051	−0.048
0.90	0.238	−2.949	+0.433	+1.00	−3.255	−0.005	−0.063	−0.060

3.5. Simulation of Optimal Treatment

In the observance of desired therapeutic window using well formulated HAART, the dynamics show that the immune system remain robust, and the exposed and infected cells together with the viral load drops to undetectable values; that is, $S = 1{,}632, E = 144, I = 19, T = 136, B = 115$ and $V \ll 1$ as shown in Figure 7.

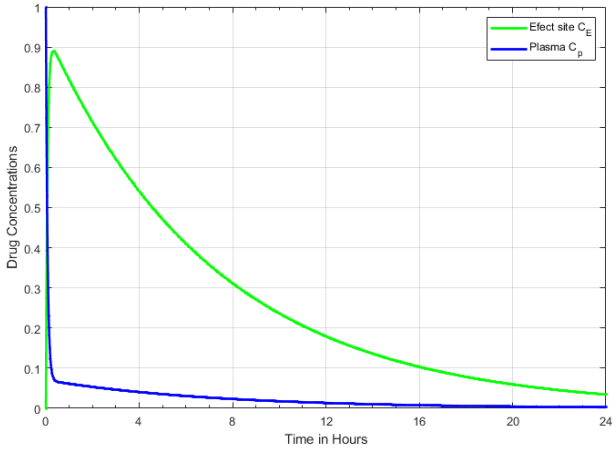

Figure 7. *Single Dose Drug Concentration at the blood plasma* $C_P(t)$ *and at the Effect site* $C_E(t)$ *in 24 hours.*

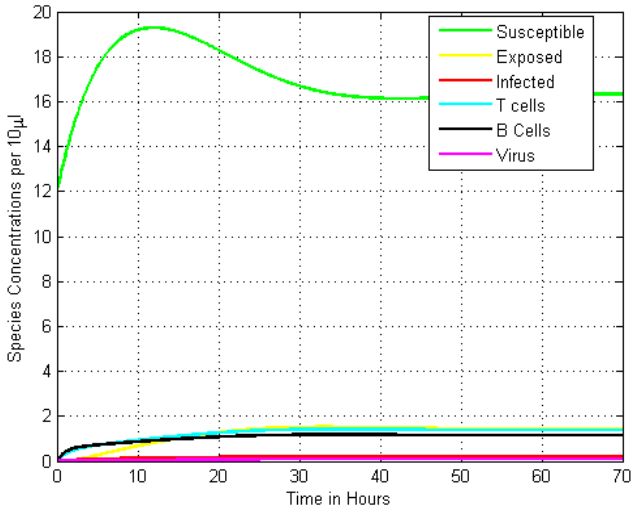

Figure 8. *Cell Population dynamics restored to almost normal at* $C_E(t) \geq 0.72$ *with persistence of viral load.*

4. Discussion

This research study used ordinary differential equations to model the in vivo dynamics of host-pathogen-drug interaction. The system of ordinary differential equations in (1) – (6) were developed from the compartmental flow chart presented in Figure 2. The focus of this study was on the immune response to viral infection in presence of HAART chemotherapy. DFE was computed and used to determine the basic reproductive ration R_0 using the next generation matrix method defined in equation (7). It was found that R_0 is a function of the control parameters $C_E, \pi, \eta, \psi, \rho$.

Elasticities of these control parameters with respect to R_0 were computed to identify the most effective control so as to guide the public health and pharmacologist's efforts in controlling the pandemic and formulating the HAART composition and administration regimen.

Using data from the literature as cited, the reproductive ratio was in absence of treatment was found to be $R_0 = 0.659$ and reduces to $R_0 = 0.239$ as the drug concentration increases to $C_E(t) = 0.9$ of dosage.

A two-compartment pharmacokinetic model was developed to determine the optimal therapeutic window, and it was estimated to be at $C_E(t) = 0.72$. At this critical therapeutic value, the elasticity of the control parameters were found to be $E_{c_e} = -1.298, E_\rho = +0.379, E_\pi = -1.573, E_\psi = -0.005, E_\eta = -0.051$ and $E_\omega = -0.048$. It is noted that the main contributors to changes in reproductive ratio is drug concentration C_E, protease inhibitors potency π which reduces the viral production (burst size), and immune cells proliferation booster ρ. The other parameters which include drug viral elimination potency ω, drug elimination of infected cells ψ and RTI preventing new infection η are relevant but of little significance.

Simulation results also indicate that observance of these parameters can reduce the viral infection to undetectable levels of $V(t) \leq 5/ml$. The B and T memory cells will be maintained at higher levels for resolution of subsequent viral invasion.

The study however did not put into the consideration the pharmacological characteristics of HAART and individual characteristics. It was assumed that concentration alone can translate to direct drug efficacy by the equation (13). Experimental measurement was not done, and therefore simulation to show comparison of model results and empirical data was not illustrated. Nevertheless, the results are biologically plausible and fall within the expected physiological range, indicating the model's realism and feasibility, and therefore the simulation results are indicative of the direction that studies can be focused and where experiments can be targeted.

5. Conclusions

This research study revealed that although the discovery of one stop treatment drug of HIV has not been discovered, the use of HAART can be of great help in boosting immunity and reducing the viral load to undetectable levels. The success of these results is based on consistency and discipline in drug administration, which calls for the innovative drug delivery mechanisms.

Abbreviations

AIDS	Acquired Immune Deficiency Syndrome
DFE	Disease Free Equilibrium
HAART	Highly Active Anti-Retroviral Therapy
HIV	Human Immunodeficiency Virus
PD	Pharmacodynamics
PI	Protease Inhibitor
PK	Pharmacokinetics
PLWHA	People Living with HIV AIDS
RTI	Reverse Transcriptase Inhibitor

Author Contributions

Paul Kipkurgat Choge: Data curation, Formal Analysis, Methodology, Writing – original draft

Titus Kiplimo Rotich: Formal Analysis, Methodology, Software, Validation, Visualization

Wesley Cheruiyot Koech: Methodology, Software, Validation, Visualization, Writing – review & editing

Data Availability Statement

The data supporting the outcome of this research work has been reported in this manuscript.

Conflicts of Interest

The authors declare no conflicts of interest.

References

[1] J.-S. Kang and M.-H. Lee, "Overview of therapeutic drug monitoring," *The Korean journal of internal medicine*, vol. 24, no. 1, p. 1, 2009. https://doi.org/10.3904/kjim.2009.24.1.1

[2] Q. Tu, M. Cotta, S. Raman, N. Graham, L. Schlapbach, and J. A. Roberts, "Individualized precision dosing approaches to optimize antimicrobial therapy in pediatric populations," *Expert Review of Clinical Pharmacology*, vol. 14, no. 11, pp. 1383-1399, 2021. https://doi.org/10.1080/17512433.2021.1961578

[3] M. Nordberg, J. Duffus, and D. M. Templeton, "Glossary of terms used in toxicokinetics (IUPAC Recommendations 2003)," *Pure and Applied Chemistry*, vol. 76, no. 5, pp. 1033-1082, 2004. https://doi.org/10.1351/pac200476051033

[4] Y. Lai *et al.*, "Recent advances in the translation of drug metabolism and pharmacokinetics science for drug discovery and development," *Acta Pharmaceutica Sinica B*, vol. 12, no. 6, pp. 2751-2777, 2022. https://doi.org/10.1016/j.apsb.2022.03.009

[5] C. Csajka and D. Verotta, "Pharmacokinetic–pharmacodynamic modelling: history and perspectives," *Journal of pharmacokinetics and pharmacodynamics*, vol. 33, pp. 227-279, 2006. https://doi.org/10.1007/s10928-005-9002-0

[6] C. B. Landersdorfer and W. J. Jusko, "Pharmacokinetic/pharmacodynamic modelling in diabetes mellitus," *Clinical pharmacokinetics*, vol. 47, pp. 417-448, 2008. https://doi.org/10.2165/00003088-200847070-00001

[7] L. Zhang, H. Xie, Y. Wang, H. Wang, J. Hu, and G. Zhang, "Pharmacodynamic parameters of pharmacokinetic/pharmacodynamic (PK/PD) integration models," *Frontiers in Veterinary Science*, vol. 9, p. 860472, 2022. https://doi.org/10.3389/fvets.2022.860472

[8] M. Ghita, C. Billiet, D. Copot, D. Verellen, and C. M. Ionescu, "Model calibration of pharmacokinetic-pharmacodynamic lung tumour dynamics for anticancer therapies," *Journal of Clinical Medicine*, vol. 11, no. 4, p. 1006, 2022. https://doi.org/10.3390/jcm11041006

[9] A. Tóth, A. Brózik, G. Szakács, B. Sarkadi, and T. Hegedüs, "A novel mathematical model describing adaptive cellular drug metabolism and toxicity in the chemo immune system," *PloS one*, vol. 10, no. 2, p. e0115533, 2015. https://doi.org/10.1371/journal.pone.0115533

[10] A. Rodríguez-Gascón, M. Á. Solinís, and A. Isla, "The role of PK/PD analysis in the development and evaluation of antimicrobials," *Pharmaceutics*, vol. 13, no. 6, p. 833, 2021. https://doi.org/10.3390/pharmaceutics13060833

[11] M. Grassi, G. Lamberti, S. Cascone, and G. Grassi, "Mathematical modeling of simultaneous drug release and in vivo absorption," *International Journal of Pharmaceutics*, vol. 418, no. 1, pp. 130-141, 2011. https://doi.org/10.1016/j.ijpharm.2010.12.044

[12] J. A. Owen, J. Punt, S. A. Stranford, and P. P. Jones, *Kuby immunology*. WH Freeman New York, 2013.

[13] N. Lam, Y. Lee, and D. L. Farber, "A guide to adaptive immune memory," *Nature Reviews Immunology*, vol. 24, no. 11, pp. 810-829, 2024. https://doi.org/10.1038/s41577-024-01040-6

[14] C. G. Whitney, F. Zhou, J. Singleton, A. Schuchat, C. f. D. Control, and Prevention, "Benefits from immunization during the vaccines for children program era-United States, 1994-2013," *MMWR Morb Mortal Wkly Rep*, vol. 63, no. 16, pp. 352-355, 2014. https://doi.org/10.15585/mmwr.mm6316a4

[15] P. Van den Driessche and J. Watmough, "Reproduction numbers and sub-threshold endemic equilibria for compartmental models of disease transmission," *Mathematical biosciences*, vol. 180, no. 1-2, pp. 29-48, 2002. https://doi.org/10.1016/S0025-5564(02)00108-6

[16] C. Moiny, E. Coussaert, and L. Barvais, "Exploring the Plasma-Effect Site Concentration Difference During Effect Site Controlled Infusion," in *On the Study and Practice of Intravenous Anaesthesia*, J. Vuyk, F. Engbers, and S. Groen-Mulder Eds. Dordrecht: Springer Netherlands, 2000, pp. 45-58. https://doi.org/10.1007/978-94-015-9604-6_4

[17] W. E. Paul, *Fundamental immunology*. Lippincott Williams & Wilkins, 2012.

[18] E. Kokuina, M. C. Breff-Fonseca, C. A. Villegas-Valverde, and I. Mora-Díaz, "Normal values of T, B and NK lymphocyte subpopulations in peripheral blood of healthy Cuban adults," *MEDICC review*, vol. 21, pp. 16-21, 2019. https://doi.org/10.37757/MR2019.V21.N2-3.5

[19] A. Saeidi *et al.*, "T-cell exhaustion in chronic infections: reversing the state of exhaustion and reinvigorating optimal protective immune responses," *Frontiers in immunology*, vol. 9, p. 2569, 2018.

[20] T. W. LeBien and T. F. Tedder, "B lymphocytes: how they develop and function," *Blood*, vol. 112, no. 5, pp. 1570-1580, 2008.

[21] R. S. Sauls, C. McCausland, and B. N. Taylor, "Histology, T-cell lymphocyte," in *StatPearls [Internet]*: StatPearls Publishing, 2023.

[22] A. Talevi and C. L. Bellera, "Compartmental pharmacokinetic models," in *ADME Processes in Pharmaceutical Sciences: Dosage, Design, and Pharmacotherapy*: Springer, 2024, pp. 173-192. https://doi.org/10.1007/978-3-031-50419-8_8

[23] K. Kuester and C. Kloft, "Pharmacokinetics of monoclonal antibodies," *Pharmacokinetics and pharmacodynamics of biotech drugs: principles and case studies in drug development*, pp. 45-91, 2006.